RAA 2015 Vol. **15** No. **12**, 2164–2172 doi: 10.1088/1674–4527/15/12/004
http://www.raa-journal.org *http://www.iop.org/journals/raa*

Research in Astronomy and Astrophysics

On the diffuse soft X-ray emission from the nuclear region of M51

Ji-Ren Liu[1] and Shu-De Mao[2,1,3]

[1] National Astronomical Observatories, Chinese Academy of Sciences, Beijing 100012, China; *jirenliu@bao.ac.cn*
[2] Physics Department and Tsinghua Center for Astrophysics, Tsinghua University, Beijing 100084, China
[3] Jodrell Bank Centre for Astrophysics, University of Manchester, Manchester, M13 9PL, UK

Received 2015 January 7; accepted 2015 May 25

Abstract We present an analysis of the diffuse soft X-ray emission from the nuclear region of M51 combining both *XMM-Newton* RGS and *Chandra* data. Most of the RGS spectrum of M51 can be fitted with a thermal model with a temperature of ~ 0.5 keV except for the O VII triplet, which is forbidden-line dominated. The Fe L-shell lines peak around the southern cloud, where the O VIII and N VII Lyα lines also peak. In contrast, the peak of the O VII forbidden line is about $10''$ offset from that of the other lines, indicating that it is from a spatially distinct component. The spatial distribution of the O VII triplet mapped by the *Chandra* data shows that most of the O VII triplet flux is located at faint regions near edges, instead of the southern cloud where other lines peak. This distribution of the O VII triplet is inconsistent with the photoionization model. Other mechanisms that could produce the anomalous O VII triplet, including a recombining plasma and charge exchange X-ray emission, are discussed.

Key words: atomic processes — plasmas — ISM: jets and outflows — galaxies: Seyfert — galaxies: individual: M51 (NGC 5194) — X-rays: ISM

1 INTRODUCTION

The Whirlpool galaxy M51 (NGC 5194) is classified as a LINER or Seyfert 2 galaxy from studies of optical emission lines (e.g., Stauffer 1982; Ho et al. 1997). The close distance of M51 (7.8 Mpc, the mean value taken from the NED[1] database) allows detailed studies of its nuclear activity. Radio observations show a bipolar outflow, comprising a southern cloud and a northern loop, which is also seen in the optical emission line map (Ford et al. 1985; Crane & van der Hulst 1992). The optical outflow with velocities as high as 1500 km s^{-1} has been reported by Cecil (1988), who also found that the arcuate radio emission of the southern cloud lies inside the bright optical emission line region, indicating a bow shock caused by the radio jet emanating from the nucleus.

The interaction between the radio jet/outflow and the surrounding gas represents an important feedback mode of an active galactic nucleus (AGN), which is crucial for our understanding of galaxy evolution (e.g. Fabian 2012). X-ray observations are very effective in studying such phenomena as

[1] *http://ned.ipac.caltech.edu*

the radio jet-driven outflow will heat the surrounding gas to X-ray emitting temperatures. Extended X-ray emission from M51 was first detected using the *Einstein Observatory* (Palumbo et al. 1985), and then with *ROSAT* (Marston et al. 1995; Ehle et al. 1995). The *BeppoSAX* data of M51 showed that X-ray emission from the nucleus is only seen directly above 10 keV, implying a neutral hydrogen column density of $N_{\rm H} \sim 10^{24}$ cm^{-2} (Fukazawa et al. 2001).

Observations by *Einstein* and *ROSAT* are limited by their spatial resolution. With its sub-arcsec angular resolution, *Chandra* has provided new insights on M51. Terashima & Wilson (2001) found that the nuclear X-ray morphology of M51 is similar to that seen in radio and optical observations. The X-ray spectra of the southern cloud and northern loop are similar and can be fitted by a thermal model with temperature ~ 0.55 keV. The X-ray morphology and spectra suggest that the nuclear X-ray emitting gas of M51 are shock-heated by the bipolar radio outflow from the nucleus. Both the X-ray point sources and the extended X-ray emission from the disk of M51 have been studied using *Chandra* (e.g., Terashima & Wilson 2004; Tyler et al. 2004) and *XMM-Newton* data (e.g., Dewangan et al. 2005; Owen & Warwick 2009).

All these X-ray studies are based on CCD data, for which the spectral resolution is around 10 at 1 keV. In contrast, the Reflection Grating Spectrometers (RGSs) aboard the *XMM-Newton* telescope (den Herder et al. 2001) have a better spectral resolution for moderately extended sources due to their large dispersion power. The RGS spectral resolution is $\sim 0.14\theta$ Å, where θ (in units of arcmin) is the angular extent of the source along the dispersion direction. For M51, the spatial extent of the nuclear X-ray emitting region is about $0.5'$, which corresponds to a spectral resolving power $\lambda/\delta_\lambda \sim 150$ at 15 Å given the spatial resolution of *XMM-Newton*. With this resolution many emission lines, especially the He-like O VII triplet which is a diagnostic tool for the thermal state of plasma, are well resolved.

The O VII triplet consists of a resonance line, two inter-combination lines and a forbidden line. For an optically-thin thermal plasma in ionization equilibrium, the electron collisional excitation is efficient and favors the resonance line. In Liu et al. (2012), we studied nine nearby star-forming galaxies (including M51) and found that the forbidden lines of their O VII triplets are comparable to or even stronger than the resonance lines. We proposed that the charge-exchange process occuring between highly ionized ions and neutral species is a possible explanation. The charge-exchange captured electrons of the recipient ions are in excited states and their downward cascading favors the forbidden line (e.g. Dennerl 2010). In the special case of M51, however, the explanation is complicated by the presence of the central low-luminosity AGN and the radio jet-driven outflow.

In Liu et al. (2012), only the line ratio of the O VII triplet of M51 was studied. In this paper we provide a more detailed study of the *XMM-Newton* RGS spectrum of M51. In particular, we study the spatial distribution of emission lines along the cross-dispersion direction of RGS.

Given this situation, the *Chandra* image of M51 with sub-arcsec angular resolution is helpful in revealing the O VII triplet distribution. Thus we also analyze the archival *Chandra* data of M51 with an accumulated exposure time of 700 ks, which is much deeper than the short exposure data (~ 15 ks) used in previous studies (e.g. Terashima & Wilson 2001).

We describe the observational data in Section 2 and present the results of *XMM-Newton* and *Chandra* data in Section 3 and Section 4, respectively. Discussion of the results is covered in Section 5. Throughout the paper, the errors quoted are for the 90% confidence level. At a distance of 7.8 Mpc, $1''$ corresponds to 38 parsec.

2 OBSERVATIONAL DATA

The two RGSs on-board the *XMM-Newton* telescope are slit-less dispersive spectrometers, and photons from extended sources are recorded on CCD detectors with the dispersion angle and 1D spatial information along the cross-dispersion direction. Because the dispersion directions are different for different observations, to ensure that the dispersed spectra are from similar spatial regions, we use

Table 1 List of *XMM-Newton* RGS observations of M51

ObsID	$t_{\rm tot}$ (ks)	$t_{\rm eff}$ (ks)	Obs time	P.A. ($^\circ$)
0212480801	49	26	2005–07–01	294
0303420101	54	35	2006–05–20	326
0303420201	37	25	2006–05–24	323
0677980701	13	13	2011–06–07	312

Notes: $t_{\rm tot}$ is the total exposure, $t_{\rm eff}$ is the useful exposure after removing periods of flares, and P.A. is the position angle.

four archival XMM-Newton RGS observations of M51 as listed in Table 1. The maximum difference in position angles between them is about 30°. The total effective exposure time is ∼100 ks after removing periods with intense flare activity.

The most recent version of the Science Analysis System (SAS 14.0) of *XMM-Newton* is used for the reduction of photon events. As stated above, the RGS spectrum is broadened by the spatial extent of the source along the dispersion direction. To produce a broadened redistribution matrix file (RMF), we convolve the RMF produced by the SAS tool *rgsproc* with a *Chandra* image of M51 (0.4–2 keV) using the *rgsrmfsmooth* tool written by Andrew Rasmussen. The broadened RMF is calculated separately for each dataset. For background subtraction, we use the model background generated by *rgsproc* based on the flux of CCD9 beyond 1′ from the on-axis position. Because M51 lies $\sim 1'$ away from the on-axis position for most observations listed in Table 1, the model background is overpredicted. Indeed, the model background exceeds the observed spectrum at $\lambda > 28$ Å. Thus we scale down the model background by a factor of 0.6 based on the event distribution of CCD9. Since we focus on emission lines, the uncertainty in the background subtraction will not affect our major results.

Because CCD4 of RGS2 covering 20–24 Å failed early in the mission, the data about the O VII triplet around 22 Å are only from RGS1. Similarly, CCD7 of RGS1 also failed and the data within 10.6–13.8 Å of RGS1 are missing. Figure 1 presents the CCD image of the *XMM-Newton* RGS data of M51 combining both RGS1 and RGS2 for all four observations. The offsets between RGS1 and RGS2 and between different observations have been corrected. The figure clearly shows the well-resolved emission lines.

We use seven *Chandra* datasets with ObsID numbers of 13812, 13813, 13814, 13815, 13816, 15496 and 15553, as observed by PI Kip Kuntz. After removing the flare periods, the total effective exposure time is about 700 ks. The datasets are analyzed with *CIAO* (version 4.6) following the standard procedures. As an illustration, Figure 2 presents the counts image of M51 within 0.4–2 keV created by merging all the seven datasets. The overplotted contours are from the radio 6 cm observation (Crane & van der Hulst 1992) and show a close correspondence with the X-ray image. The *XMM-Newton* RGS dispersion direction is also illustrated in Figure 2.

3 XMM-NEWTON RGS RESULTS

3.1 Spatial Distribution of X-ray Emission Lines

First we study the spatial distribution of the well-resolved X-ray emission lines along the cross-dispersion direction of *XMM-Newton* RGS. The Fe XVII lines at 15 and 17 Å, the O VIII and N VII Lyα lines at 19 and 24.8 Å respectively, and the O VII forbidden line at 22.1 Å are studied. The corresponding wavelength regions adopted to calculate the photon counts are 14.8–15.5, 16.6–17.4, 18.6–19.4, 24.4–25.2 and 21.8–22.4 Å, respectively. We find that the profiles of Fe XVII lines at 15 and 17 Å are similar, as are the O VIII and N VII Lyα lines. For clarity, only the profiles of the Fe XVII line at 15 Å, O VIII Lyα line at 19 Å, and O VII line at 22.1 Å are plotted in Figure 3. We see that the bright Fe XVII line at 15 Å is centrally peaked around 50″, with a full width at half maximum

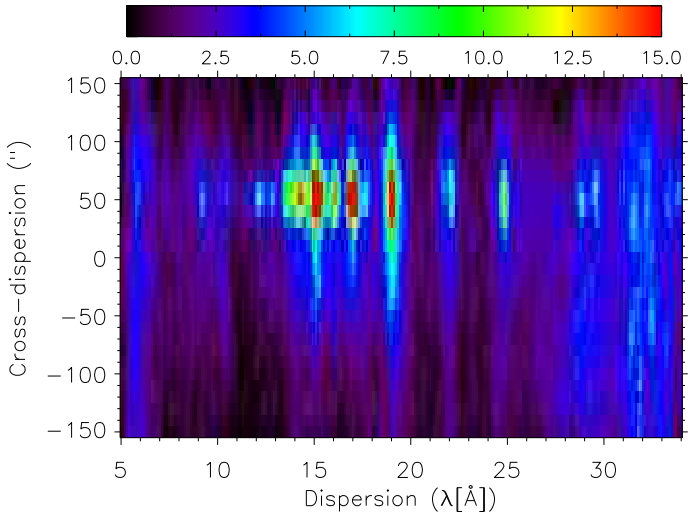

Fig. 1 CCD image showing the cross-dispersion vs dispersion of M51 combining both RGS1 and RGS2 data from all four observations. The emission lines are seen as vertical contours and are well resolved. The color bar is for the total event counts on a linear scale. The zero point along the cross-dispersion direction of ObsID 0303420201 is adopted.

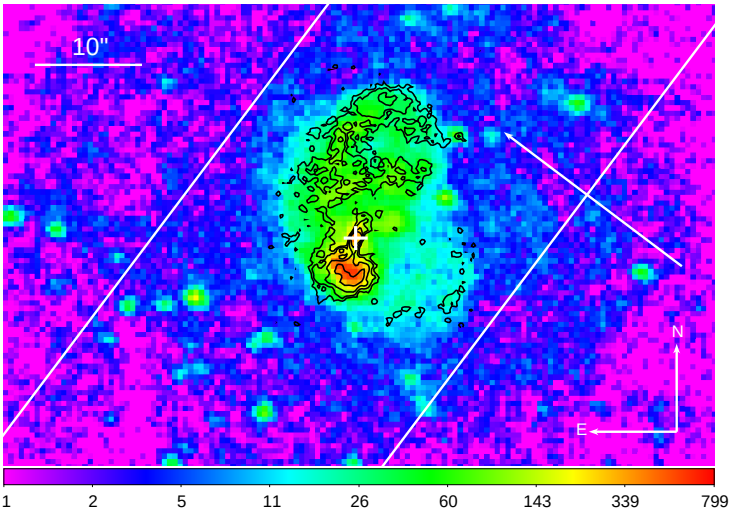

Fig. 2 *Chandra* counts image of M51 within 0.4–2 keV (logarithmically scaled). The overlaid radio contours (1.5, 3, 6 and 12 in units of 10 μJy) are from VLA observations at a wavelength of 6 cm by Crane & van der Hulst (1992). The two solid lines separated by 30″ indicate the RGS dispersion direction of ObsID 0303420201, while the arrow indicates the positive cross-dispersion direction. The white cross marks the position of the nucleus of M51, which corresponds to a cross-dispersion distance of 52″ for ObsID 0303420201.

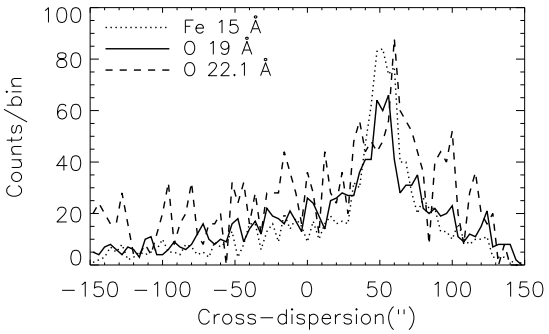

Fig. 3 Spatial distribution of the emission lines of Fe XVII at 15 Å, O VIII Lyα at 19 Å, and O VII forbidden line at 22.1 Å. For clarity, the profile of the O VII forbidden line at 22.1 Å has been multiplied by a factor of 4.

(FWHM) of $\sim 20''$. This FWHM is similar to the spatial resolution of *XMM-Newton* RGS. Since the cross-dispersion position of $50''$ corresponds to the location of the southern cloud, it means that the emission lines of Fe XVII are mainly from the compact southern cloud.

The O VIII Lyα line at 19 Å is also peaked around $50''$, the same as the Fe XVII lines. The spatial distribution of the O VII forbidden line at 22.1 Å is, however, different from those of the other lines. Its maximum is around $60''$, $10''$ offset from the peaks of other lines. This indicates that the O VII forbidden line is from a spatially distinct component, compared with the other lines.

3.2 X-ray Spectrum of M51

Since the X-ray emission lines have different spatial distributions, it is optimal to extract spectra within different spatial regions. However, a difference of $\sim 10''$ in the scale is too small to allow such spectral extractions from *XMM-Newton* RGS. Thus we only extract one spectrum centered on the nucleus of M51 with a cross-dispersion width of about $1'$. The background-subtracted spectrum of M51 combined from both RGS1 and RGS2 data of all four observations is plotted in Figure 4.

We see that the spectrum of M51 is dominated by emission lines. The O VII triplet is dominated by the forbidden line at 22.1 Å and the N VI triplet also has a forbidden line comparable with its resonance line. The bright Fe L-shell lines around 15–17 Å indicate that they are not from a photoionized plasma, for which the Fe L-shell lines are expected to be much weaker (e.g., Kallman et al. 1996; Sako et al. 2000). They are likely due to a collisionally ionized plasma as suggested in previous studies (e.g., Terashima & Wilson 2001). Thus we fit an optically thin collisional-ionization-equilibrium (CIE) thermal model (vapec, Foster et al. 2012) to the observed RGS spectrum of M51. Only the abundances of the elements of Ne, Fe, O and N, which show bright emission lines in the spectrum of M51, are allowed to vary. The abundances of other elements are set to solar values (Lodders 2003).

On the other hand, the forbidden-line dominated O VII triplet of M51 shows a spatial distribution different from other lines. As stated in Section 1, it is impossible to explain such an anomalous triplet by a thermal CIE model. Thus we add two Gaussians to represent the O VII resonance and forbidden lines. The intercombination line is too weak to be fitted. Similarly, we add another two Gaussians to represent the N VI resonance and forbidden lines. The model is subject to an absorption model of *wabs* (Morrison & McCammon 1983) with a foreground neutral hydrogen column density of 2×10^{20} cm^{-2} (Kalberla et al. 2005). The fitted results are listed in Table 2 and overplotted in Figure 4.

Table 2 Fitting Results

T (keV)	N	O	Ne	Fe	O VII$_r$	O VII$_f$	N VI$_r$	N VI$_f$	χ^2_ν
0.52 ± 0.02	4.4 ± 1.1	0.6 ± 0.1	0.6 ± 0.2	0.3 ± 0.1	1.3 ± 0.7	4.1 ± 1.0	2.2 ± 0.9	2.5 ± 1.2	0.91

Notes: the abundances are relative to the solar values; O VII$_{r,f}$ and N VI$_{r,f}$ (in units of 10^{-5} photons s^{-1} cm^{-2}) are the line intensities of the O VII resonance line, the O VII forbidden line, the N VI resonance line, and the N VI forbidden line, respectively.

The model provides a reasonable fit to the observed spectrum of M51. The fitted temperature is 0.52 keV, similar to that obtained by Terashima & Wilson (2001). However, the fitted abundances are higher than their measured values, which are only around 0.1 solar value. The low abundances they obtained are most likely due to the poor spectral resolution of *Chandra* data. We note that the fitted O and N abundances are not affected by the Gaussian fitting to the corresponding O VII and N VI triplets, since they are most likely due to a mechanism different from CIE models and at the fitted temperature, the emissivity of O VII and N VI triplets of the CIE model is weak. The residuals around the Fe and O lines are likely due to the simple convolution modeling of the RMF. There are residuals around 13.5 Å, indicating that the Ne X triplet is underestimated. The residuals around 18.6 Å are likely due to the O VII Heβ line.

The temperature diagnostic G ratio of the He-like triplet for a thermal CIE plasma is defined as (Gabriel & Jordan 1969)

$$\mathrm{G} = \frac{\mathrm{f} + \mathrm{i}}{\mathrm{r}}, \tag{1}$$

where f, i and r represent the intensity of the forbidden, intercombination, and resonance lines, respectively. If we assume the intensity of the intercombination line is 1/4 that of the forbidden line (Smith et al. 2001), the fitted G ratio of the O VII triplet is 3.9 ± 2.3. Similarly, the fitted G ratio of the N VI triplet is 1.4 ± 0.8. The G ratio of the O VII triplet shows that the O VII triplet is not due to CIE thermal plasmas, for which the G ratios are generally smaller than 1. The G ratio of the N VI triplet is barely consistent with a CIE model around 10^6 K.

4 *Chandra* RESULTS

As shown in Section 3.1, the peak of the spatial profile of the O VII forbidden line is offset from those of other lines by $\sim 10''$. This scale can be easily resolved with *Chandra* data. Thus we analyze the *Chandra* data of M51 in this section.

We use the contour binning method (Sanders 2006) to divide the nuclear X-ray emitting region of M51 into 34 different bins with a minimum signal to noise ratio of 40. The X-ray spectrum is extracted from each bin with a background spectrum taken from a source-free region outside the nuclear region. We fit a thermal CIE model with variable O, Ne, Mg and Fe abundances and limit the fitting range to 0.4–1.5 keV. We include a Gaussian (with a center of 21.85 Å and a width of 0.25 Å) to represent the O VII triplet. Adding a Gaussian will improve the χ^2 by 4.3 on average. The improvement of χ^2 is 8.1 for the spectra with the Gaussian line fluxes larger than 5×10^{-7} photons s^{-1} cm^{-2}. We also tested the fitting method by fitting mock spectra with a line flux of 1×10^{-6} photons s^{-1} cm^{-2}, and found that about 75% of the fitted fluxes are within 3 sigma of the true value.

Due to the limited spectral resolution of *Chandra* data, we do not expect the fitted O VII triplet fluxes to be as accurate as the measurement by the *XMM-Newton* RGS data. Nevertheless, it is likely to provide a qualitative distribution of the O VII triplet, especially for bins with high O VII triplet fluxes. The fitted fluxes of the O VII triplet from the *Chandra* data are plotted in the left panel of Figure 5. For comparison, an image showing the binned counts is plotted in the right panel. We see that the fluxes of the O VII triplet are generally higher for faint bins near the edges. It shows that the

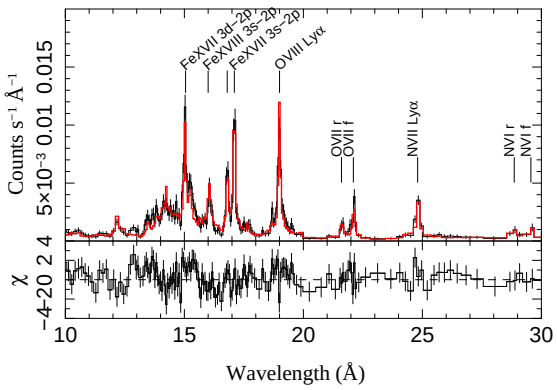

Fig. 4 Background-subtracted *XMM-Newton* RGS spectrum of M51 combining both RGS1 and RGS2 data of all four observations. Red histograms are the fitted thermal model with four Gaussians. χ is the difference between data and model divided by the error.

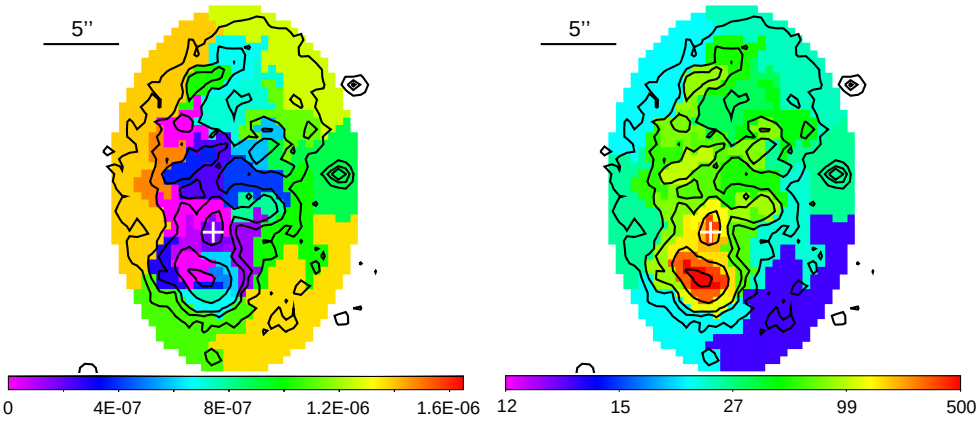

Fig. 5 *Left*: Fluxes of the O VII triplet obtained with the *Chandra* data of M51 using the contour binning method. *Right*: The binned counts map of M51 within 0.4–2 keV. The contours of levels 20, 50, 80, 200 and 550 for the unbinned map are plotted in both panels. The white cross marks the nucleus of M51.

fitted O VII triplet has a more extended distribution than that of the total emission within 0.4–2 keV, which is centered on the southern cloud. The northern regions have more O VII triplet flux than the southern part. This is consistent with the *XMM-Newton* result. Another interesting feature to note is that the southern cloud seems to be enclosed by an arc of the O VII triplet in the outward direction.

5 DISCUSSION

We have analyzed the *XMM-Newton* RGS spectrum of M51, the emission lines of which are well resolved. Most of the spectrum of M51 can be fitted by a thermal CIE model with temperature ~ 0.5 keV, except for the O VII triplet, which is forbidden-line dominated. The Fe XVII lines at 15 and

17 Å are centrally peaked around the cross-dispersion position of 50″ with an FWHM of 20″. This indicates that they are mainly from the compact southern cloud. The O VIII Lyα line at 19 Å and N VII Lyα line at 25 Å also peak around the same position as the Fe XVII lines. In contrast, the peak of the O VII forbidden line is about 10″ offset from the other lines. The O VII triplet map obtained with the *Chandra* data shows that most of the fluxes of the O VII triplet are located in faint regions, instead of the southern cloud around which other lines peak.

As stated in Section 1, the forbidden-line-dominated O VII triplet of M51 cannot be due to a thermal CIE plasma, and we have proposed the charge-exchange process as a possible explanation. Nevertheless, the existence of a low-luminosity AGN and the radio jet-driven outflow in the nuclear region of M51 makes other explanations possible, including photoionization and non-equilibrium-ionization plasmas. Below we discuss them in turn.

For a photoionized plasma, the emission is dominated by recombination, which also favors the forbidden line. One characteristic feature of the photoionization model is the spatial profile. As the central AGN is the ionizing source, the ionizing flux will decline as r^{-2} and photoionization is most important for regions close to the AGN. This has been illustrated by the optical study of M51 (Bradley et al. 2004), which shows that photoionization is dominant within the inner region ($r < 1''$) and the shock model is preferred outside it ($r \sim 2.5''$). The mapped morphology of the O VII triplet from *Chandra* data shows no fluxes around the nucleus and is most prominent at the outer regions. This is inconsistent with the photoionization model.

All the optical, radio and X-ray studies of M51 support a scenario in which the nuclear gas of M51 is shock-heated by the radio outflow emanating from the nucleus (Cecil 1988; Ford et al. 1985; Terashima & Wilson 2001). In this situation, the non-equilibrium-ionization (NEI) plasma is another possible explanation for the anomalous O VII triplet. If a plasma is shock-heated suddenly, the ionization process lags behind heating, and will result in an ionizing plasma. The inner-shell collisional ionization of O^{5+} ions can lead to excited O^{6+} ions and enhance the forbidden line emission (e.g., Liedahl 1999). However, this only happens in a short transition period when the O^{5+} fraction is non-negligible. Using the *Sedov* model (Borkowski et al. 2001), we find that the G ratio of the O VII triplet is around 3 at an ionization time $n_e t \sim 3.5 \times 10^9$ cm^{-3}s. This timescale is too short compared with the spatial extent we studied. A more likely explanation is a recombining NEI plasma.

When a blast wave expands into a rarefied medium, a recombining plasma could be produced due to rapid adiabatic cooling, as proposed to explain the radiative recombination continuum features in some supernova remnants (e.g., Yamaguchi et al. 2012). The spatial distribution of the O VII triplet mapped by the *Chandra* data is consistent with this scenario. A unique test of a recombining plasma is the associated radiative recombination continuum. However, due to the presence of strong Fe lines, it is hard to tell whether there is a radiative recombination continuum of O VII (at 16.8 Å) in the spectrum of M51.

On the other hand, to explain the anomalous O VII triplet with the charge-exchange process, the interacting interfaces between the highly ionized gas and neutral species are needed. The observed HI (Walter et al. 2008) and CO (Koda et al. 2011) maps of M51 are well correlated with the spirals. CO is detected around the nucleus (e.g. Matsushita et al. 2007) and shown to be aligned with the radio emission. Different from the recombining plasma, the charge-exchange model shows no radiative recombination continuum, but has enhanced emission lines from preferred energy levels ($n = 4 - 7$ for O VII) (e.g. Beiersdorfer et al. 2003). Future spatially-resolved high-resolution X-ray spectroscopy by the soft X-ray spectrometer of Astro-H will be able to test the existence of the radiative recombination continuum of M51.

Acknowledgements We thank the referee for their valuable comments and Lijun Gou and Richard Long for reading the draft. This work is supported by a National Natural Science Foundation of China for Young Scholar Grant (11203032), and by the Strategic Priority Research Program

"The Emergence of Cosmological Structures" of the Chinese Academy of Sciences Grant No. XDB09000000 and NSFC grant 11333003 (SM). This research has made use of *XMM-Newton* archival data. *XMM-Newton* is an ESA science mission with instruments and contributions directly funded by ESA Member States and the USA (NASA). In addition, the research used observations obtained with the *Chandra* X-ray observatory, which is operated by the Smithsonian Astronomical Observatory on behalf of NASA.

References

Beiersdorfer, P., Boyce, K. R., Brown, G. V., et al. 2003, Science, 300, 1558
Borkowski, K. J., Lyerly, W. J., & Reynolds, S. P. 2001, ApJ, 548, 820
Bradley, L. D., Kaiser, M. E., & Baan, W. A. 2004, ApJ, 603, 463
Cecil, G. 1988, ApJ, 329, 38
Crane, P. C., & van der Hulst, J. M. 1992, AJ, 103, 1146
den Herder, J. W., Brinkman, A. C., Kahn, S. M., et al. 2001, A&A, 365, L7
Dennerl, K. 2010, Space Sci. Rev., 157, 57
Dewangan, G. C., Griffiths, R. E., Choudhury, M., Miyaji, T., & Schurch, N. J. 2005, ApJ, 635, 198
Ehle, M., Pietsch, W., & Beck, R. 1995, A&A, 295, 289
Fabian, A. C. 2012, ARA&A, 50, 455
Ford, H. C., Crane, P. C., Jacoby, G. H., Lawrie, D. G., & van der Hulst, J. M. 1985, ApJ, 293, 132
Foster, A. R., Ji, L., Smith, R. K., & Brickhouse, N. S. 2012, ApJ, 756, 128
Fukazawa, Y., Iyomoto, N., Kubota, A., Matsumoto, Y., & Makishima, K. 2001, A&A, 374, 73
Gabriel, A. H., & Jordan, C. 1969, MNRAS, 145, 241
Ho, L. C., Filippenko, A. V., & Sargent, W. L. W. 1997, ApJS, 112, 315
Kalberla, P. M. W., Burton, W. B., Hartmann, D., et al. 2005, A&A, 440, 775
Kallman, T. R., Liedahl, D., Osterheld, A., Goldstein, W., & Kahn, S. 1996, ApJ, 465, 994
Koda, J., Sawada, T., Wright, M. C. H., et al. 2011, ApJS, 193, 19
Liedahl, D. A. 1999, in Lecture Notes in Physics, Berlin Springer Verlag, 520, X-Ray Spectroscopy in Astrophysics, ed. J. van Paradijs & J. A. M. Bleeker, 189
Liu, J., Wang, Q. D., & Mao, S. 2012, MNRAS, 420, 3389
Lodders, K. 2003, ApJ, 591, 1220
Marston, A. P., Elmegreen, D., Elmegreen, B., et al. 1995, ApJ, 438, 663
Matsushita, S., Muller, S., & Lim, J. 2007, A&A, 468, L49
Morrison, R., & McCammon, D. 1983, ApJ, 270, 119
Owen, R. A., & Warwick, R. S. 2009, MNRAS, 394, 1741
Palumbo, G. G. C., Fabbiano, G., Trinchieri, G., & Fransson, C. 1985, ApJ, 298, 259
Sako, M., Kahn, S. M., Paerels, F., & Liedahl, D. A. 2000, ApJ, 543, L115
Sanders, J. S. 2006, MNRAS, 371, 829
Smith, R. K., Brickhouse, N. S., Liedahl, D. A., & Raymond, J. C. 2001, ApJ, 556, L91
Stauffer, J. R. 1982, ApJS, 50, 517
Terashima, Y., & Wilson, A. S. 2001, ApJ, 560, 139
Terashima, Y., & Wilson, A. S. 2004, ApJ, 601, 735
Tyler, K., Quillen, A. C., LaPage, A., & Rieke, G. H. 2004, ApJ, 610, 213
Walter, F., Brinks, E., de Blok, W. J. G., et al. 2008, AJ, 136, 2563
Yamaguchi, H., Ozawa, M., & Ohnishi, T. 2012, Advances in Space Research, 49, 451